

# Non-uniform Incident Illumination Effect on the Thermal Performance of Low Concentrating Multi-Junction Solar Cells

Fahad G. Al-Amri

Department of Basic Engineering, College of Engineering, University of Dammam, P.O. Box 1982, Dammam 31441, Saudi Arabia, fgalamri@uod.edu.sa

## Abstract

The modern multi-junction concentrating solar cell is an emerging technology that is expected to play a crucial role in achieving solutions to energetic and environmental challenges that the world faces today. A potential technical limit to widespread adoption of this technology is the degradation of solar cell efficiency at high operating temperatures. In this paper, a numerical heat transfer model is presented and applied to determine the effects of non-uniform incident illumination on the operating temperature of a triple-junction solar cell. Results show that even at quite low solar concentrations, maximum solar cell temperature significantly increased in the presence of non-uniform incident light, causing hot spots in some portions of the cell. Thus, a conventional cooling system, such as a plain channel, is insufficient for operating solar cells at reasonable temperatures under non-uniform illumination. However, the non-uniformity of the incident radiation has no effect on bulk fluid temperature and collected thermal energy at the duct exit.

**Keywords:** Concentration solar cell; non-uniform illumination profile; active cooling; conjugate convection; surface radiation

## 1. Introduction

The incident light on the surface of a concentrating solar cell is strongly non-uniform (Baig et al., 2012). As a result, the majority of light is intensified onto a small area of the cell surface, causing a hot spot in this part of cell. This in turn causes a current mismatch and degradation in the overall efficiency of the CPV. Several researchers have investigated the effect of non-uniform incident light on electrical performance (Franklin and Coventry, 2003), but few have studied the thermal impact of the problem.

The experimental study by Coventry et al. (2002) showed that a silicon solar cell under non-uniform incident illumination has less open-circuit voltage and efficiency compared to a cell under uniform light. Domenech-Garret (2011) explored the influences of a combination of non-uniform illumination and non-uniform temperature on a silicon solar cell. Gaussian and inverse Gaussian profiles were used to describe the temperature in the cell, which simulated a general cell cooling device. Chemisana and Rosell (2011) investigated, both numerically

and experimentally, the effects of Gaussian and anti-Gaussian temperature profiles on the electrical performance of the cell under various types of concentrated radiation. They found that electric conversion efficiency increases under a Gaussian temperature profile and decreases when the cell is subjected to an inverse Gaussian temperature curve. They concluded that the temperature profile could be tailored to maximize efficiency under determined radiation conditions. Al-Amri and Mallick (2014) investigated the combined effects of surface radiation and forced convection on the concentrating triple-junction solar cell temperature under non-uniform illumination and at medium solar concentration. They found that surface radiation exchanged inside the channel reduced cell temperature. Recently, Xing et al. (2016) studied the electrical and thermal performances of a silicon triple-junction solar cell under non-uniform light. As the degree of non-uniformity increased, a remarkable increment in cell temperature was observed.

It is well observed and documented in the literature that the cooling of PV panels increase the electrical efficiency of such systems. Presently several PV cooling methodologies exist that include active water and air cooling and passive techniques such as PCM cooling, conductive cooling, etc (Kumar & Rosen, 2011). The passive cooling techniques have an advantage of using natural means to provide cooling yet such systems are comparatively larger in size, need higher capital investment and have complex

maintenance. This limits the applicability of passive cooling system. On the contrary, plain channel air/water cooling is still far better than the others because of its simplicity, smaller size, less capital investment and easy maintenance although they require electrical input for continuous operation (Grubisic-Cabo et al. 2016).

To the best of our knowledge, at low solar concentrations, the non-uniformity effect of the incident light has not been investigated. Therefore, in this study, a numerical model was developed to determine the temperature distribution on the low concentrating solar cells under non-uniform incident illumination. The results of this work will aid estimation of the overall efficiency of a CPV system and assessment of the adequacy of a conventional cooling system in maintaining cell temperatures below the acceptable limit.

## 2. Mathematical Formulations

The triple-junction solar cell employed in this work consisted of three semiconducting materials, gallium indium phosphide (GaInP), gallium arsenide (GaAs), and germanium (Ge), each absorbing a different spectrum of incident light, and a front contact, Cu-Ag-Hg, for capturing the generated current. It was attached to a front cover glass and a rear aluminum duct via adhesives (see Figure 1). The properties and dimensions of these components can be found elsewhere (Al-Amri and Mallick, 2013). The duct walls were considered to be gray, opaque, and diffuse surfaces, and the inlet and exit areas were

considered to be black surfaces. In addition, it was assumed that the external wall was adiabatic, that air flow entered at a constant velocity ( $u_\infty$ ), that ambient temperature was constant, that cell conversion efficiency ( $\eta$ ) was 0.38, and that reflectivity was 0.85 for the front metal contact and zero for all other cell components. The illumination distribution incident on the concentrating cell surface was strongly non-uniform and took the shape of a Gaussian profile (Franklin and Conventry, 2003). Therefore, the formula of the light intensity adopted in the current model was:

$$I(z) = \frac{2C}{10^4 SD \sqrt{2\pi}} e^{-\frac{2(z-z_0)^2}{S^2}} \quad (1),$$

where  $z_0$  is the position of the maximum illumination on the cell surface, and  $S$  is the standard deviation of the illumination, measuring how far the illumination is spread out.

The intensity of incident light  $I(z)$  can be written in the non-dimensional form as:

$$\bar{I}(Z) = \frac{I(z)}{I_{avg}} \quad (2),$$

where  $I_{avg}$  is the average incident illumination across the entire cell surface.

The physical problem under consideration is governed by the energy conservation equation in solid regions and the equations of energy, continuity, and momentum in fluid regions under the constraint of radiation equations along each of the two channel walls. These equations can be written under usual boundary assumptions (Al-Amri and Mallick, 2013).

*Continuity equation*

$$\frac{\partial V}{\partial Y} + \frac{\partial U}{\partial Z} = 0 \quad (2)$$

*Momentum equation*

$$V \frac{\partial U}{\partial Y} + U \frac{\partial U}{\partial Z} = \frac{dP}{dZ} + \frac{G_r^*}{Re} (\theta - \theta_\infty) + \frac{\partial^2 U}{\partial Y^2} \quad (3)$$

*Energy equation fluids*

$$V \frac{\partial \theta_f}{\partial Y} + U \frac{\partial \theta_f}{\partial Z} = \frac{1}{Pr} \frac{\partial^2 \theta_f}{\partial Y^2} \quad (4)$$

*Energy equation for each solid material*

$$\frac{\partial^2 \theta_s}{\partial Y^2} = 0 \quad (5)$$

The integral form of the continuity equation was also utilized to solve the problem (Al-Amri, 2008; Al-Amri and El-Shaarawi, 2010):

$$F = \int_0^1 U dY = 1 \quad (6)$$

The surface radiation exchanges inside the channel are determined by applying the first law of thermodynamic per unit surface area on the channel plate element (Al-Amri, 2008; Al-Amri and El-Shaarawi, 2010), yielding the following two constraint equations:

*Surface 1 ( $Y = 0$ )*

$$N_{rad} \theta_\infty^4 \left[ \frac{1}{2} - \left( \frac{Z Re}{2} \right) \left( 1 + Z^2 Re^2 \right)^{-\frac{1}{2}} \right] + N_{rad} \theta_e^4 \left[ \frac{1}{2} - \left( \frac{(L-Z) Re}{2} \right) \left( 1 + (L-Z)^2 Re^2 \right)^{-\frac{1}{2}} \right]$$

$$\begin{aligned}
 & + \int_0^L \left\{ \frac{1-\varepsilon_2}{\varepsilon_2} \left( \frac{\partial \theta_f}{\partial Y} \Big|_{Y=1^-} - \frac{\partial \theta_s}{\partial Y} \Big|_{Y=1^+} \right) + N_{\text{rad}} \theta_{w2}^4(Z) \right\} \\
 & \left[ 1 + \text{Re}^2(Z-Z')^2 \right]^{(-3/2)} \frac{\text{Re}}{2} dZ' = - \frac{1-\varepsilon_1}{\varepsilon_1} \frac{\partial \theta_f}{\partial Y} \Big|_{Y=0^+} \\
 & + N_{\text{rad}} \theta_{w1}^4(Z) - \frac{\partial \theta_f}{\partial Y} \Big|_{Y=0^+} \quad (7),
 \end{aligned}$$

where  $N_{\text{rad}} = \sigma q_{\text{avg}}^3 \frac{b^4}{k_f^4}$ .

Surface 2 ( $Y = 1$ )

$$\begin{aligned}
 & \text{KR}_{s1-f} \frac{\partial \theta_s}{\partial Y} \Big|_{Y=1^+} + N_{\text{rad}} \theta^4 * \\
 & \left[ \frac{1}{2} - \left( \frac{Z \text{Re}}{2} \right) \left( 1 + Z^2 \text{Re}^2 \right)^{\frac{1}{2}} \right] \\
 & + N_{\text{rad}} \theta_e^4 \left[ \frac{1}{2} - \left( \frac{(L-Z) \text{Re}}{2} \right) \left( 1 + (L-Z)^2 \text{Re}^2 \right)^{\frac{1}{2}} \right] \\
 & + \int_0^L \left\{ \frac{1-\varepsilon_1}{\varepsilon_1} \left( - \frac{\partial \theta}{\partial Y} \Big|_{Y=0^+} \right) + N_{\text{rad}} \theta_{w1}^4(Z) \right\} \\
 & * \frac{1}{2} \left[ 1 + \text{Re}^2(Z-Z')^2 \right]^{(-3/2)} \text{Re} dZ' = \frac{1-\varepsilon_2}{\varepsilon_2} \left[ \frac{\partial \theta_f}{\partial Y} \Big|_{Y=1^-} - \right. \\
 & \left. N_{\text{rad}} \theta_{w2}^4(Z) - \frac{\partial \theta_f}{\partial Y} \Big|_{Y=1^-} \right] \quad (8)
 \end{aligned}$$

When surface radiation is absent (i.e.,  $\varepsilon = 0$ ), equations (6) and (7) are reduced to:

$$\frac{\partial \theta_f}{\partial Y} \Big|_{Y=0} = 0 \quad (9)$$

$$\text{KR}_{s1-f} \frac{\partial \theta_s}{\partial Y} \Big|_{Y=1^+} = \frac{\partial \theta_f}{\partial Y} \Big|_{Y=1^-} \quad (10)$$

Dimensionless boundary conditions must be defined.

At the channel entrance ( $Z = 0$  and  $0 < Y < 1$ ):  
 $U = 1, V = P = 0$ , and  $\theta = \theta_\infty$  (11a)

At the first wall of the channel ( $Z > 0$  and  $Y = 0$ ):  
 $U = V = 0$  (11b)

At the second wall of the channel ( $Z > 0$  and  $Y = 1$ ):  $U = V = 0$  (11c)

At the solid-solid interface of the solar cell assembly, for  $Z > 0, Y = Y_{m(i)-(i+1)}$ , and  $i = 1$  or 2:

$$\frac{\partial \theta_s}{\partial Y} \Big|_{Y=Y_{m(i)-(i+1)}^-} = \text{KR}_{m(i+1)-i} \frac{\partial \theta_s}{\partial Y} \Big|_{Y=Y_{m(i)-(i+1)}^+}$$

For  $Y = Y_{m(i)-(i+1)}, 0 < Z < Z_c$  or  $(Z_c + L_c) < Z < L$ , and  $i = 3$  or 4:

$$\begin{aligned}
 & \frac{\partial \theta_s}{\partial Y} \Big|_{Y=Y_{m(i)-(i+1)}^-} = \text{KR}_{m(i+1)-i} \frac{\partial \theta_s}{\partial Y} \Big|_{Y=Y_{m(i)-(i+1)}^+} \\
 & + \frac{(1-\eta) \alpha_{m_i} (1 - \alpha_{m_8} - \alpha_{m_7}) \bar{I}(Z)}{\text{KR}_{m_i-f}}
 \end{aligned}$$

For  $Y = Y_{m5-7}$  and  $0 < Z < Z_c$  or  $(Z_c + L_c) < Z < L$ :

$$\begin{aligned}
 & \frac{\partial \theta_s}{\partial Y} \Big|_{Y=Y_{m5-7}^-} = \text{KR}_{m7-5} \frac{\partial \theta_s}{\partial Y} \Big|_{Y=Y_{m5-7}^+} + \\
 & \frac{(1-\eta) \alpha_{m_5} (1 - \alpha_{m_8} - \alpha_{m_7}) \bar{I}(Z)}{\text{KR}_{m5-f}} \Big|_{Y=1^+}
 \end{aligned}$$

For  $Y = Y_{m(i)-(i+1)}, Z_c \leq Z \leq (Z_c + L_c)$ , and  $i = 3, 4$ , or 5:

$$\frac{\partial \theta}{\partial Y} \Big|_{Y=Y_{m(i)-(i+1)}^-} = \text{KR}_{m(i+1)-i} \frac{\partial \theta}{\partial Y} \Big|_{Y=Y_{m(i)-(i+1)}^+}$$

For  $Y = Y_{m6-7}$  and  $Z_c \leq Z \leq (Z_c + L_c)$ :

$$\frac{\partial \theta}{\partial Y} \Big|_{Y=Y_{m_{6-7}}^-} = kR_{m_{7-6}} \frac{\partial \theta}{\partial Y} \Big|_{Y=Y_{m_{6-7}}^+} + \frac{\alpha_{m_6} (1 - \alpha_{m_8} - \alpha_{m_7}) \bar{I}(Z)}{kR_{m_{6-f}}}$$

For  $Z > 0$  and  $Y = Y_{m_{7-8}}$  :

$$\frac{\partial \theta}{\partial Y} \Big|_{Y=Y_{m_{7-8}}^-} = kR_{m_{8-7}} \frac{\partial \theta}{\partial Y} \Big|_{Y=Y_{m_{7-8}}^+} + \frac{\alpha_{m_7} (1 - \alpha_{m_8}) \bar{I}(Z)}{kR_{m_{7-f}}}$$

For  $Z > 0$  and  $Y = Y_{m_8}$  :

$$\frac{\partial \theta}{\partial Y} \Big|_{Y=Y_{m_8}} = \frac{\alpha_{m_8} \bar{I}(Z)}{kR_{m_{8-f}}}$$

In each case,  $kR_{m_{(i+1)-i}} = \frac{k_{m_{i+1}}}{k_{m_i}}$  and  $kR_{m_i-f} = \frac{k_{m_i}}{k_f}$

### 3. Method of Solution

The conjugate convection equations (continuity, momentum, and energy) are solved using a finite difference numerical marching technique while the two radiation constraint equations are solved iteratively using the Gauss-Seidel method. As a first iteration, the continuity, momentum, and energy equations, subject to the boundary conditions (Equations 9-11), are solved assuming that surface radiation is absent. The obtained solution is then utilized to solve the radiation constraint equations to update the temperature. These updated temperatures are used as new boundary conditions to resolve the convection equations. These procedures are repeated until convergence is achieved. Details of this method of solution and

validation of the code can be found elsewhere (Al-Amri, 2008; Al-Amri and El-Shaarawi, 2010).

### 4. Results and Discussion

Temperature distribution on a solar cell surface is influenced by parameters related to the optical system, such as concentration ratio (C), the degree of non-uniformity of the incident light (as described by the S), and parameters related to the cooling system, such as the Reynolds number (Re) and channel wall emissivity ( $\epsilon$ ). In this study, the effects of three parameters (S,  $\epsilon$ , and C) on cell temperature were investigated. Figure 2 illustrates how the solar cell temperature varies with the axial distance from the channel entrance for both uniform and non-uniform incident light at three values of S (0.0005, 0.001, and 0.002). Results show that when distribution is uniform, the solar cell temperature increases until reaching its maximum value at the channel exit. This maximum is less than 75°C, indicating that the triple-junction solar cell can be operated with acceptable conversion efficiency. However, when the distribution is non-uniform, the temperature profile takes the shape of a Gaussian distribution, and the maximum temperature occurs where maximum illumination occurs on the cell surface. In this case, the maximum temperature is extremely elevated relative to that seen with uniform light distribution. The lower the S, the higher the maximum temperature. Figure 3 shows the temperature distribution on the solar cell surface for three values of

emissivity, highlighting a small noticeable drop in maximum solar cell temperature as emissivity increases while the balance of the cell surface is nearly unchanged. This means that the effect of surface radiation on temperature distribution is negligible at low values of  $C$ , the opposite of what is seen at

higher values (Al-Amri and Mallick, 2014, 2013).

Figures 4 and 5 show, for  $S = 0.0005$ ,  $z_0 = 0.5$ ,  $Re = 500$ , and  $\epsilon = 0.95$ , the variations in cell temperature with axial distance from the channel entrance at three values of  $C$  and for non-uniform and uniform light profiles,

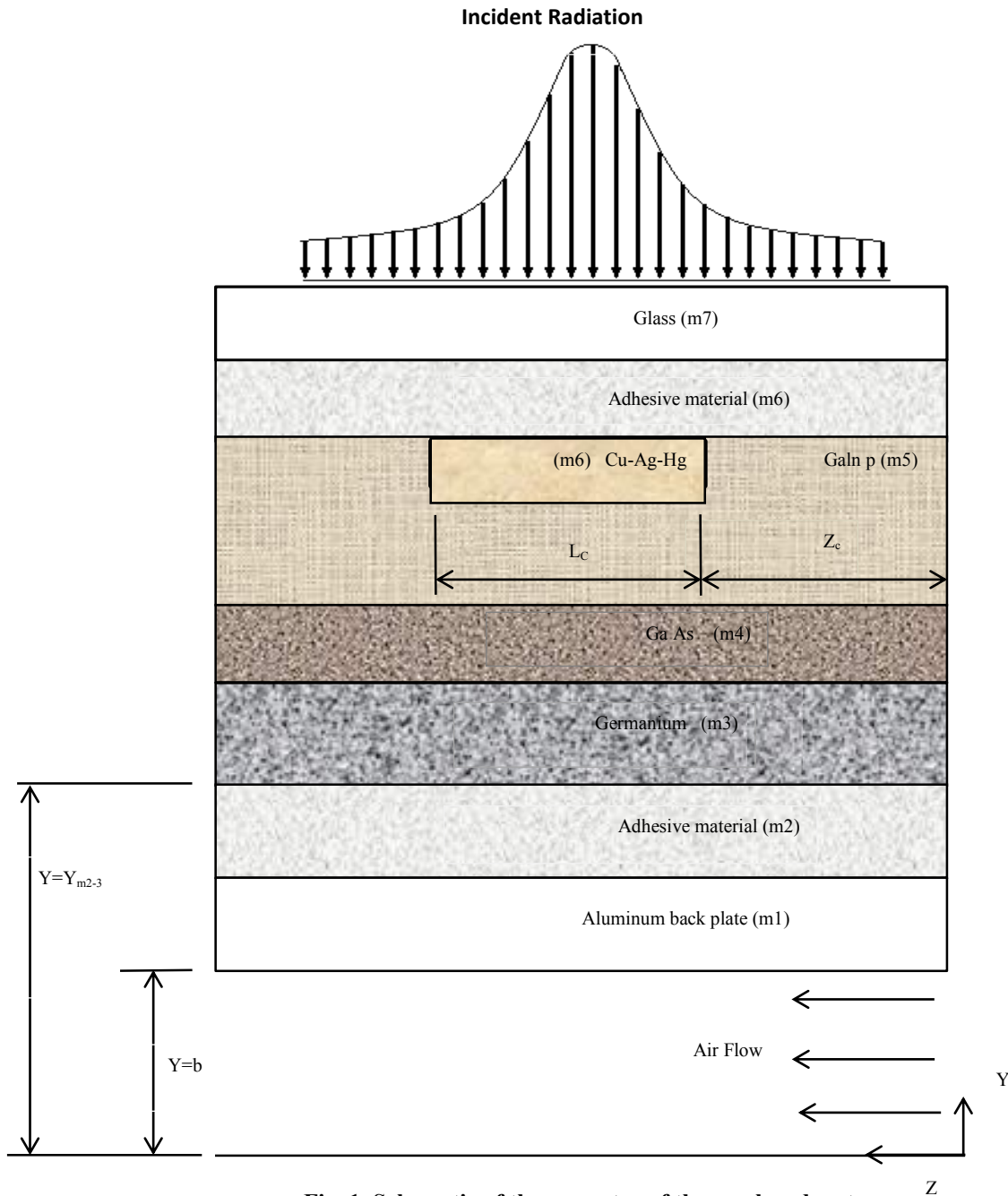


Fig. 1. Schematic of the geometry of the employed system.

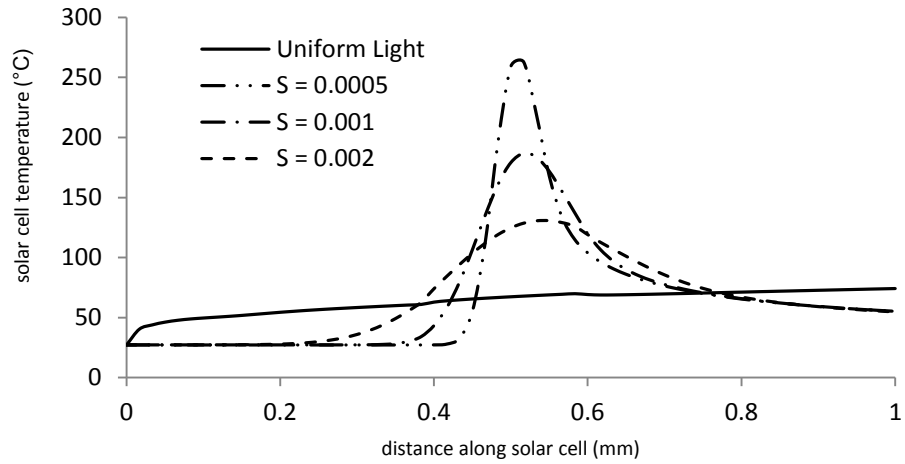


Fig. 2. Variations in solar cell temperature at various values of  $S$  when  $z_0 = 0.5$ ,  $Re = 500$ ,  $\varepsilon = 0.95$ , and  $C = 30$ .

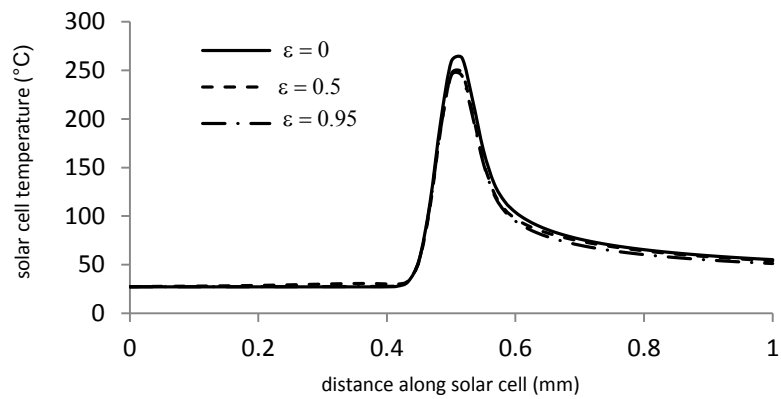


Fig. 3. Variations in solar cell temperature at various values of  $\varepsilon$  when  $S = 0.0005$ ,  $z_0 = 0.5$ ,  $Re = 500$ , and  $C = 30$ .

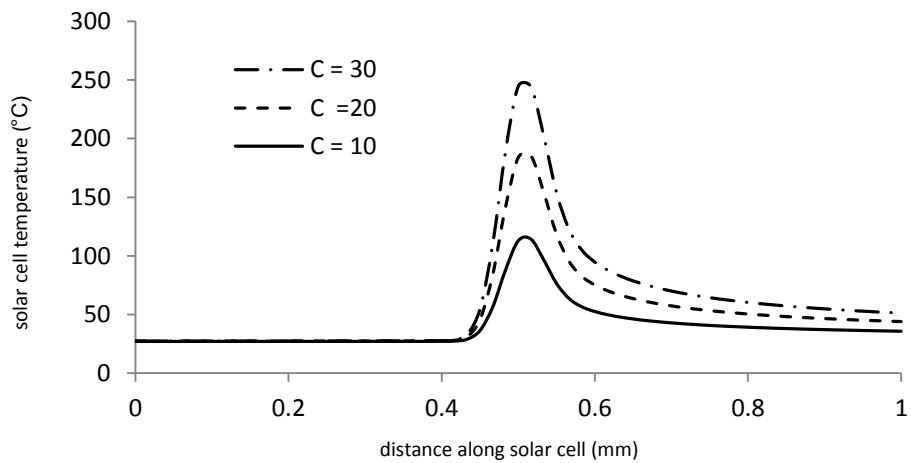


Fig. 4. Variations in solar cell temperature at various values of  $C$  when  $S = 0.0005$ ,  $z_0 = 0.5$ ,  $Re = 500$ , and  $\varepsilon = 0.95$ .

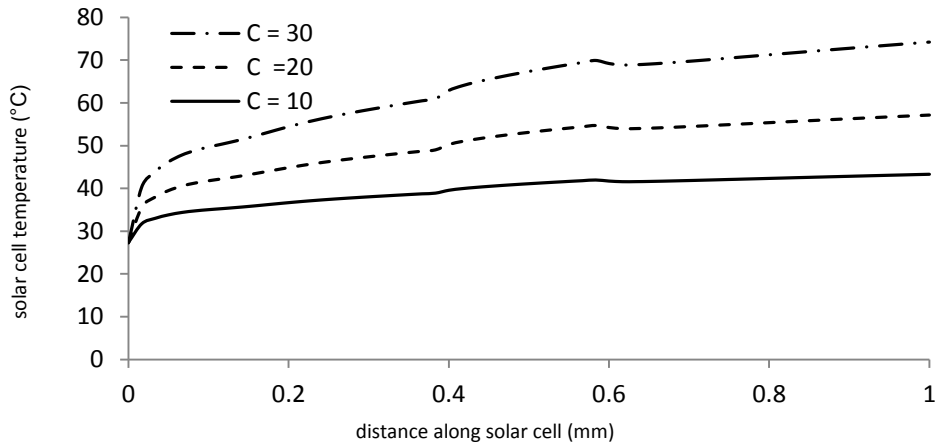


Fig. 5. Variations in solar cell temperature at various values of C when  $S = 0.0005$ ,  $z_0 = 0.5$ ,  $Re = 500$ , and  $\varepsilon = 0.95$ .

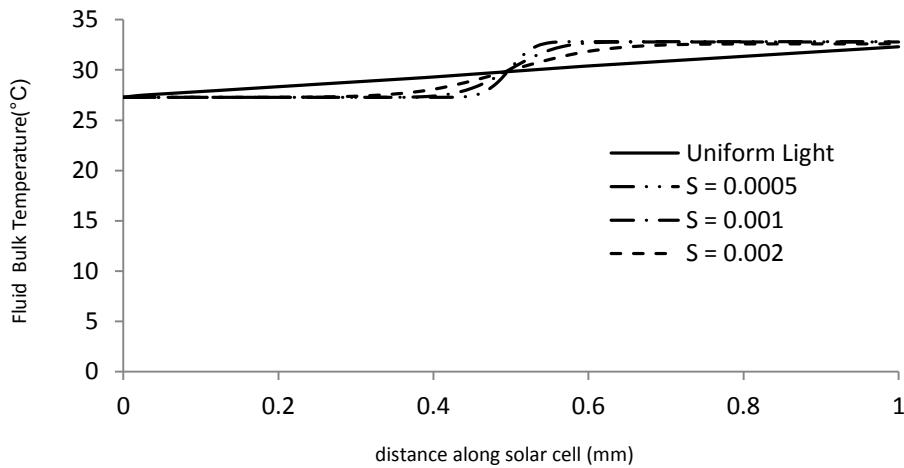


Fig. 6. Variations in fluid bulk temperature at various values of SD when  $z_0 = 0.5$ ,  $Re = 500$ ,  $\varepsilon = 0.95$ , and  $C = 30$ .

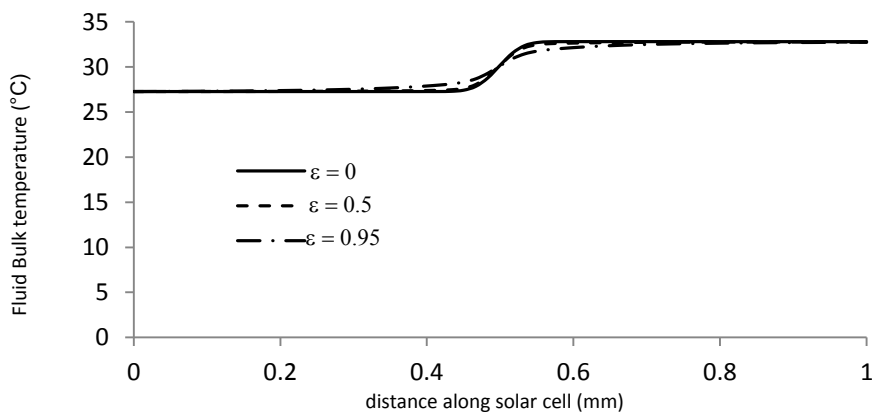


Fig. 7. Variations in fluid bulk temperature at various values of  $\varepsilon$ , when  $SD = 0.0005$ ,  $z_0 = 0.5$ ,  $Re = 500$ , and  $C = 30$ .

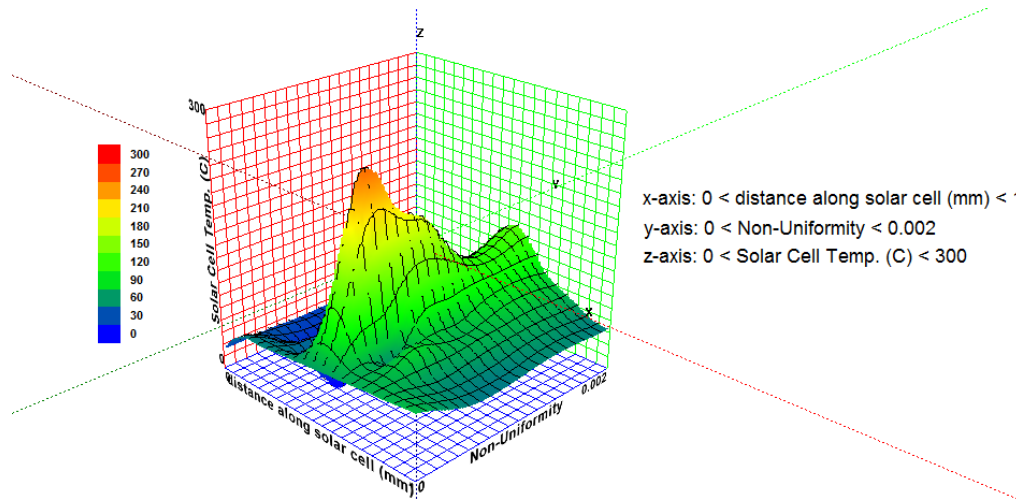


Fig. 8. 3-D Plot of Solar Cell Temperature as a Non-Linear Function of S along the length of solar cell.

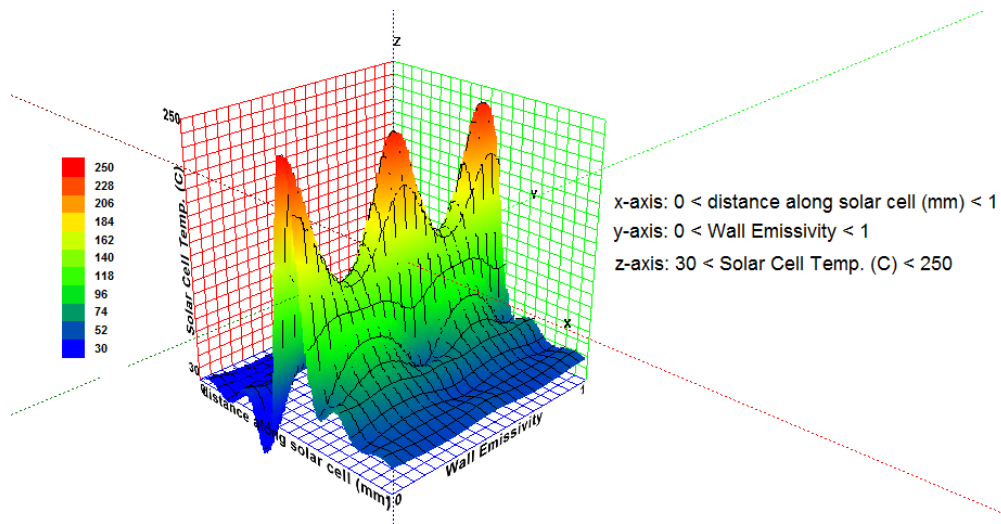


Fig. 9. 3-D Plot of Solar Cell Temperature as a Non-Linear Function of  $\epsilon$  along the length of solar cell.

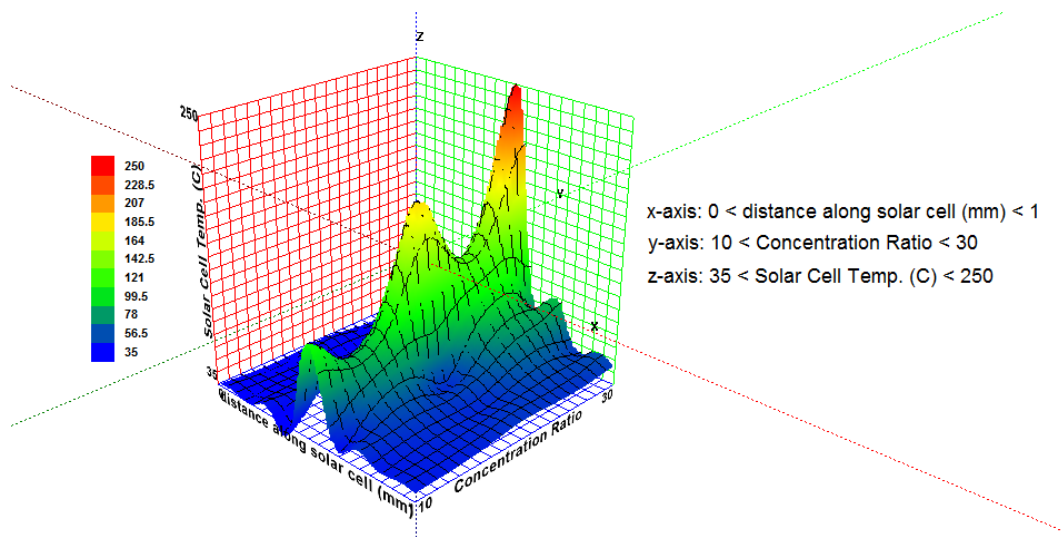


Fig. 10. 3-D Plot of Solar Cell Temperature as a Non-Linear Function of C along the length of solar cell.

respectively. It is obvious from the figures that maximum temperature increases significantly with  $C$ . Specifically, as  $C$  increased from 10 to 30 (i.e., by 200%) the maximum solar cell temperature increased by approximately 114% and 72% under non-uniform and uniform light, respectively. In addition, when the light distribution is non-uniform (Figure 5), the maximum temperature was above  $100^{\circ}\text{C}$  even when the concentration ratio was as low as 10, indicating that under non-uniform light distribution, a conventional plain channel is not appropriate for cooling the cell, even at low values of  $C$ .

Figure 6 shows the variation of fluid bulk temperature with the axial distance from the duct entrance under various incident illumination profiles. Results reveal that the shape of the incident light visibly affects the fluid bulk temperature profile inside the channel. However, the effect of the incident radiation profile on the fluid bulk temperature at the duct exit is insignificant. Figure 7 illustrates the emissivity effect of the two duct walls on the fluid bulk temperature. Surface radiation was found to have an insignificant effect on the fluid bulk temperature; therefore, it can be neglected. The effect of junction hotspot and temperature rise as a Non-Linear Function of the Three Parameters ( $S$ ,  $\epsilon$ ,  $C$ ) are shown in 3-D Plots given by figures 8, 9 & 10 respectively

## 5. Conclusions

When this numerical heat transfer model is used to simulate the temperature distribution

on a concentrated solar cell under non-uniform incident radiation at low values of  $C$ , non-uniformity strongly alters the temperature distribution in the solar cell, causing hot spots in some regions. Maximum solar cell temperature increases as  $SD$  or  $C$  increases. However, surface radiation exchange inside the channel has only a slight effect on the solar cell temperature. In addition, plain channel cooling is inadequate for cooling the solar cell, even at low values of  $C$ . Although in the current study, the non-uniformity of the incident radiation was assumed to be normally distributed however, in practice, it is possible to have Biased Distribution Model which could be positively or negatively skewed due to varying shadowing/cloudy conditions. Still the results of the current study will be valid while the temperature distribution and location of hot spots would be shifted based on the skewness of the illumination distribution model.

## References

- Baig, H, Heasman, K. C., Mallick, T. K., 2012. Non-uniform Illumination in Concentrating Solar Cells, *Renewable Sustainable Energy Reviews* 16, pp 5890-5909.
- Franklin, E., Conventry, J., 2003. "Effect of highly non-uniform illumination distribution on electrical performance of solar cell," *Proceedings of Solar, Australian and New Zealand Solar Energy Society*.
- Conventry, J., Franklin, E., Blakers, A., 2002.

- “Thermal and electrical performance of a concentrating PV/thermal collectors: Result from ANU CHAPS collector,” 40th Conference of the Australia and New Zealand Solar Energy Society, Newcastle., Domenech-Garret, J-L., 2011. Cell Behavior Under Different Non-uniform Temperature and Radiation Combined Profiles Using a Two Dimensional Finite Element Model, Solar Energy 85, pp 256-265.
- Chemisana, D., Rosell, J., 2011. Electrical performance increase of concentrator solar cells under Gaussian temperature profiles, Progress in Photovoltaics: Research and Applications.
- Al-Amri, F., Mallick, T., 2014. Effects of Non-uniform Incident Illumination on the Thermal Performance of a Concentrating Triple Junction Solar Cell, International Journal of Photoenergy, Article ID 642819.
- Xing, Y., Zhang, K., Zhao, J., Han, P., 2016. Thermal and Electrical Performance Analysis of Silica Vertical Multi-Junction Solar Cell under Non-uniform Illumination, Renewable Energy, 90, pp 77-82.
- Al-Amri, F., Mallick, T. K., 2013. Alleviating Operating Temperature of Concentration Solar Cell by Air Active Cooling and Surface Radiation, Applied Thermal Engineering, 59, pp 348-354.
- Al-Amri, F., 2008. “Effect of surface radiation on internal flows with non-isothermal boundary conditions,” PhD Dissertation, King Fahd University of Petroleum & Minerals, Dhahran, Saudi Arabia.
- Al-Amri, F. G., El-Shaarawi, M. A. I., 2010. Combined Forced Convection and Surface Radiation Between Two Parallel Plates,” International Journal of Numerical Methods for Heat and FluidFlow, 20, pp 218–239.
- Grubisic-Cabo, F. Nizetic, S. Marco, T., 2016. Photovoltaic Panels: A Review of the Cooling Techniques, Transactions of Famena XL- Special Issue 1. Pp 63-74.
- Kumar, R., Rosen, M.A., 2011. A critical review of photovoltaic-thermal solar collectors for air heating, Applied Energy, 88, pp 3603-3614.

### Nomenclature

b	channel width, m
C	concentration ratio
Gr*	modified Grashof number, $\frac{g\beta q_{avg} b^4}{\nu^2 K_f}$
I	intensity of incident light, W/m <sup>2</sup>
k	thermal conductivity, W/m · K
ℓ	channel length, m
L	dimensionless plate length, $\frac{\ell}{b Re}$
p	pressure of fluid at any cross section, N/m <sup>2</sup>
p'	pressure defect at any cross section, p - p <sub>s</sub> , N/m <sup>2</sup>
p <sub>s</sub>	hydrostatic pressure, -ρ <sub>∞</sub> gZ, N/m <sup>2</sup>
p <sub>∞</sub>	pressure of fluid at the channel entrance, N/m <sup>2</sup>
P	dimensionless pressure at any cross section, $\frac{p' - p_{\infty}}{\rho_{\infty} u_{\infty}^2}$

$N_{rad}$	radiation number, $\sigma q_{avg}^3 b^4 / k_f^4$	$\theta_{\infty}$	dimensionless inlet temperature at any
$q_{avg}$	average input heat flux, $(1 - \eta) I_{avg}$ ,	point	$\left[ \frac{k_f T_{\infty}}{q_{avg} b} \right]$
$W/m^2$		$\varepsilon$	wall emissivity
Re	Reynolds number, $\frac{u_o b}{\nu}$	$\sigma$	Stefan Boltzman constant, $5.67 \cdot 10^{-8}$
t	solar cell assembly thickness, m	$W/m^2 k^4$	
T	temperature at any point, K	<u>Subscripts</u>	
$T_{\infty}$	inlet temperature, K	c	Cu-Ag-Hg front contact
SD	standard deviation	e	exit
$u_{\infty}$	entrance axial velocity, m/s	f	fluid
u	longitudinal velocity component at any	m	material
point, m/s		s	solid
U	dimensionless longitudinal velocity, $u /$	w	wall of the channel
$u_{\infty}$		$\infty$	ambient or inlet
v	transverse velocity component at any point,	1	duct wall at $Y = 0$
m/s		2	duct wall at $Y = 1$
V	dimensionless transverse velocity, $b * v /$		
$\nu$			
y	horizontal coordinate, m		
Y	dimensionless horizontal coordinate, $y / b$		
z	vertical coordinate, m		
$z_0$	position of the maximum incident light,		
m			
Z	dimensionless vertical coordinate, $z / (b$		
* Re)			

Greek Symbols

$\nu$	kinematic fluid viscosity
$\rho$	fluid density, $kg/m^3$
$\mu$	dynamic fluid viscosity, $kg/m \cdot s$
$\alpha$	absorptivity
$\eta$	efficiency of the solar cell
$\theta$	dimensionless temperature at any point

$$\left[ \frac{k_f T}{q_{avg} b} \right]$$



